

Supplemental Information

Intercalation of Solvated Na-ions into Graphite

Lukas Seidl,^{1, 2, 3, 4} Nicolas Bucher,⁵ Eileen Miao Ling Chu,³ Steffen Hartung,⁵ Sladjana Martens,^{2, 3, 4}
Oliver Schneider^{2, 3, 4} and Ulrich Stimming^{1, 2, 3, 4, 5, 6}

^aPhysik-Department, Technische Universität München, James-Franck Straße 1, 85748 Garching

^bInstitut für Informatik VI, Technische Universität München, Schleißheimerstraße 90a, 85748 Garching

^cElectrochemical Research Group, Technische Universität München, Schleißheimerstraße 90a, 85748 Garching, Germany

^dJoint Research Institute for Advanced Power Sources for Electric Vehicles, Technische Universität München, 85748 Garching, Germany, Tsinghua University, 100084 Beijing, China

^eTUM CREATE, 1 CREATE Way, #10-02 CREATE Tower, Singapore 138602, Singapore

^fSchool of Chemistry, Newcastle University, Newcastle Upon Tyne NE1 7RU, United Kingdom

1. Experimental

Electrolytes

Electrolytes were prepared by dissolving NaClO₄ (Sigma Aldrich ACS reagent, ≥ 98.0 %) in ethylene glycol dimethyl ether (G₁, Sigma Aldrich, anhydrous, 99.5 %), diethylene glycol dimethyl ether (G₂, Sigma Aldrich, anhydrous, 99.5 %), triethylene glycol dimethyl ether (G₃, Alfa Aesar, 99 %), tetraethylene glycol dimethyl ether (G₄, Sigma Aldrich, ≥ 99 %) as well as in a 1:1 (volume) mixture of ethylene carbonate (EC, Sigma Aldrich, anhydrous, 99 %) and dimethyl carbonate (DMC, Sigma Aldrich, anhydrous, ≥ 99 %). Before use, the electrolytes were dried using 3 Å molecular sieves (Merck Millipore) for several days, which lowered the water content of all electrolytes well below 40 ppm (checked via Karl-Fischer titration measurements, Metrohm).

Electrochemistry

Cyclic voltammetry (CV) and galvanostatic charge/discharge experiments were performed in three electrode stainless steel Swagelok® cells with a mesocarbon microbead (MCMB, TB-17) working electrode (WE, 10 mm diameter) coated on a Cu-foil and a metallic Na foil (Sigma Aldrich, 99.9 %) reference (RE, 6 mm diameter) and counter electrode (CE, 10 mm diameter). As in this study a Na counter electrode was used, the term “discharge” in the following relates to sodium intercalation into graphite, while “charge” corresponds to de-intercalation. In an actual battery device with graphite as the negative material this assignment of charge/discharge would be opposite. As the measurements are carried out in three electrode configuration, the electrochemical data shown are not affected by the choice of the counter electrode. For the electrode coating an ink composed of 90 %_{wt} MCMB as active material and 10 %_{wt} PVDF (Kynar 900 HSV) binder were mechanically ground in a mortar under addition of a NMP (Merck EMPLURA®, ≥ 99.5 %, Sigma Aldrich, anhydrous, 99.5 %) solvent. The obtained slurry was coated onto the Cu-foil, before the NMP was evaporated at 50 °C. 10 mm

electrodes were punched from this coating and pressed with 1 bar pressure between two polished stainless steel stamps (Mauthe Maschinenbau, KBr-press PE-011). Before cell assembly, the electrodes were vacuum dried at 120 °C for 2 h (Büchi Glass Oven B585) and transferred into an Ar-filled (Westfalen, 5.0) glovebox (MBRAUN, MB 200 B glovebox and MB 20G LMF gas purifier). The O₂- and the H₂O-content of the glovebox did not exceed levels of 1 ppm. In the Swagelok® cell the WE was separated from the CE by four to eight glass fibre separators (VWR collection, particle retention: 1.6 µm), while each separator was soaked with 40 µl of electrolyte. Long-term battery tests severely suffered from dendrite formation between WE and CE upon charging. In order to prevent short cuts this large number of separators was necessary. The RE was connected to the cell via another separator. Gamry® potentiostats (Interface 100) with the Gamry Instruments Framework Data Acquisition Software (Version 6.25) were used for the battery tests.

XRD

For the *in-operando* XRD measurements a Rigaku SmartLab X-ray diffractometer (200 mA, 45 kV) was operated in reflection mode with a Cu_{Kα} X-ray source. The electrochemical cell is specifically designed for *in-operando* XRD measurements and described elsewhere.¹ Here, the MCMB powder was mixed with 10 to 20 %_wt teflonised acetylene black (TAB), before it was pressed with 2 t pressure onto a stainless steel grid, which was separated with a glass fibre (Whatman) separator from the Na-metal CE. The electrode was vacuum dried at 120 °C before use. A 6 µm thin Al-foil (Goodfellow, light tight) served as XRD window.

STM

STM measurements were conducted on HOPG (Highly Oriented Pyrolytic Graphite, MikroMasch ZYB), which was freshly cleaved with adhesive tape before use. The HOPG was operated as WE (0.125 cm²) in a Teflon-made electrochemical cell, while the RE and CE were made from metallic Na. The STM-tip was a mechanically cut Pt/Ir-wire (80/20, MaTeck) coated with molten polypropylene (300°C) of a pipette tip (Eppendorf eP.T.I.P.S.® Standard, polypropylene). It is worth mentioning that the used electrolytes dissolve standard insulation materials for EC-STM like polyethylene or Apiezone® wax, resulting in too high Faradaic currents. The custom made microscope system is composed of a PicoSPM STM base (Agilent Technologies®, formerly Molecular Imaging®) with a Pico STM S scanner and a Nanoscope IIIA controller (Veeco Instruments Inc.®). It is combined with an EC-Tec bipotentiostat/galvanostat BP600 and an EC-Tec biscangenerator SG600. The microscope was operated with the Nanoscope v5.31.r1 software and the potentiostats were controlled and read out with a labview® program BP600. STM data was evaluated with the WSxM software.²

EQCM

An Agilent E5100A network analyser with an in-house developed Delphi software was used to read out the admittance of the 10 MHz AT cut quartz resonators (KVG Quartz Crystal Technology) in EQCM measurements. The quartzes have a keyhole shaped Au-electrode on each crystal side, where one electrode served as WE. For the measurements, the WE electrode contact was connected via an inductor to the potentiostat (Ivium Technologies CompactStat®) and at the same time via a capacitor to the signal output connector of the network analyser. The second gold electrode that was not in contact with the electrolyte was directly connected to the network analyser signal input connector via a shielded BNC cable. Before measurements, a short circuit ("Thru") calibration was carried out in the frequency range relevant for the measurements. The WE was coated with a thin film of graphite (C-ENERGY SFG 6 L GRAPHITE, Imerys Graphite & Carbon Switzerland Ltd.) with an airbrush gun (Sparmax AC-55). For the coating a SFG6:PVDF (8:2) NMP-ink was prepared. The coating itself was done on a ca. 60 °C to 80 °C hotplate, which helped to evaporate the NMP quickly, leading to a more homogenous

coating. Since only the keyhole shaped Au-electrodes should be coated, the remaining quartz was covered with a nail polish during coating. The nail polish could be easily removed without leaving any residues after coating. The thickness of the coating needs to be chosen such that the Q-factor (signal intensity to signal width ratio) of the quartz resonator is still good enough for a reliable analysis and the electrochemical pattern in the CV is still recognizable. Thus, typical graphite loadings on the quartz were in the range of several $10 \mu\text{g cm}^{-2}$ (estimated from Sauerbrey's equation³ by comparing admittance spectra in air recorded before and after coating). The quartz was finally mounted into a Teflon cell, which was sealed with Simriz™ O-rings and filled with 300 μl of electrolyte. Na-metal served as CE and RE. After cell assembly, the cell was closed with a Teflon lid to prevent significant solvent evaporation. Afterwards, electrochemical measurements were carried out as described in Section 3.5 of the main paper, and the admittance spectra were recorded in parallel. After the end of the experiments, all admittance spectra were fitted using a Levenberg-Marquard algorithm to a Lorentz function, from which the resonance frequency f and the damping w were taken and correlated, based on measurement time, to the electrochemical data points. Typically, for each measurement, the change in resonance frequency $\Delta f(t) = f(t) - f(t=0)$ and in analogous manner of the damping $\Delta w(t)$ were calculated.

2. Supporting Results

2.1. Electrochemistry

Figure SI 1 shows voltage profiles of the first 20 charge/discharge cycles of MCMB in all tested electrolytes ((a) – (d)) and the corresponding capacities and coulombic efficiencies plotted versus the cycle ((e) – (h)). The black dots at cycle 10 in Figure SI 1 (e) to (h) show over which range the measured capacities usually scatter from experiment to experiment.

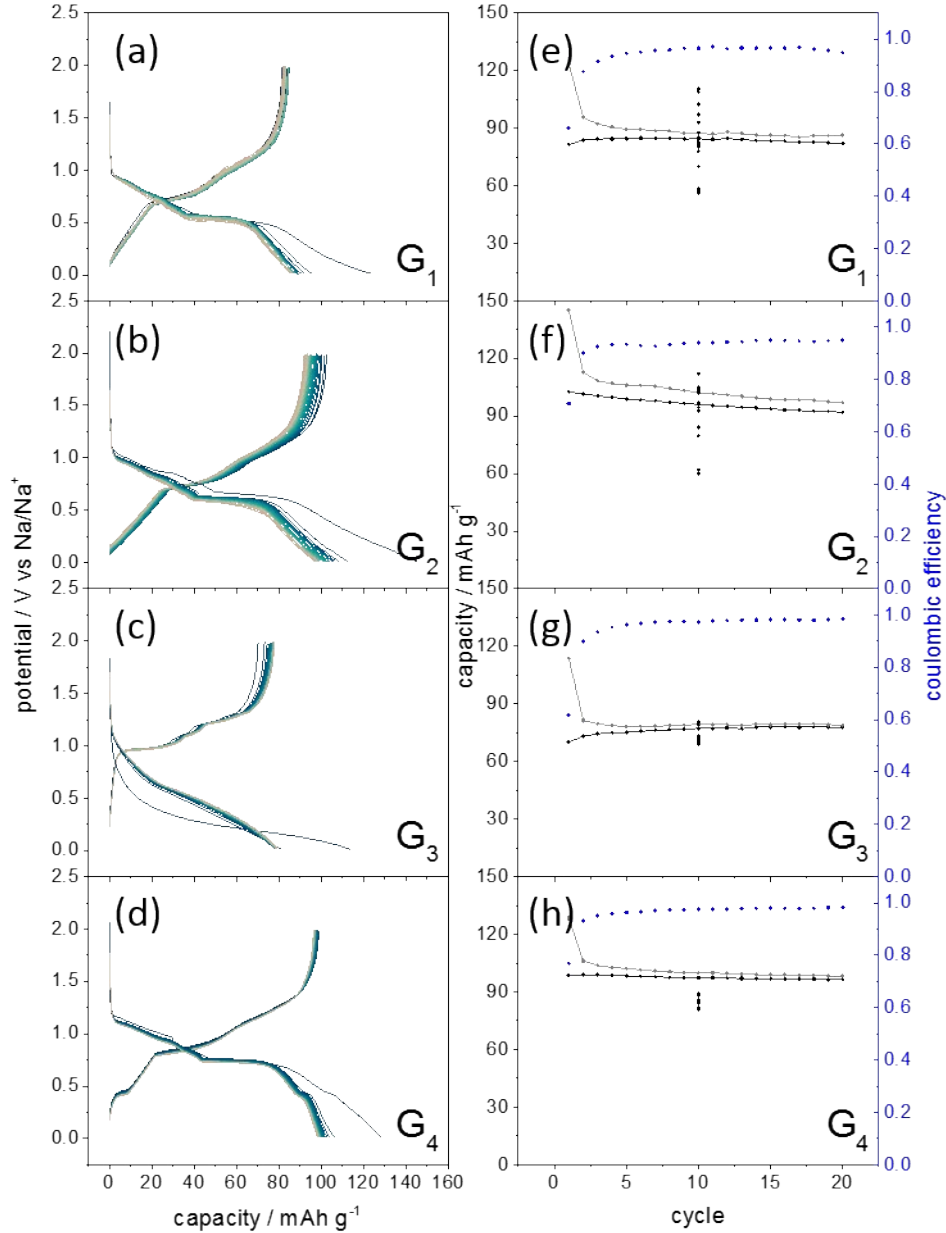


Figure SI 1: Voltage profiles measured at 50 mA/g of MCMB in 1 M NaClO₄ in (a) G₁, (b) G₂, (c) G₃ and (d) G₄ with the corresponding charge (black)/discharge (grey) capacities and coulombic efficiencies (blue) in (e) G₁, (f) G₂, (g) G₃ and (h) G₄.

The measured capacity allows to determine the stoichiometry of the formed Na-GIC: the capacity of the first discharge in the G₁-electrolyte (Figure 2 (a) in the main document) amounts to 95.7 mAh g⁻¹, which equals to 344.5 As g⁻¹. Since only one electron per Na-ion with the elemental charge of $1.602 \cdot 10^{-19}$ As is transferred upon intercalation, $2.15 \cdot 10^{21}$ Na⁺ g⁻¹ are intercalated into the Na-GIC, while 1 g of graphite ($M = 12.011$ g mol⁻¹) contains $5.01 \cdot 10^{22}$ C-atoms. Thus, the ratio of C-atoms to Na-atoms is 23.3, which gives a stoichiometry of ca. NaC₂₃. For the other electrolytes one measures capacities of 112.8 mAh g⁻¹ (G₂), 73.2 mAh g⁻¹ (G₃) and 106.3 mAh g⁻¹ (G₄), which results in the stoichiometries NaC_{19.8} (G₂), NaC_{30.4} (G₃) and NaC₂₁ (G₄). Similarly, the stoichiometries of the partially sodiated graphite were calculated from the corresponding capacity values before the main intercalation peak (for G₁, G₂ and G₄), or after the main deintercalation peak (for G₃).

Figure SI 2 compares the CVs of the third cycles of a MCMB electrode cycled in 1 M NaClO₄ in the different glymes, *i.e.* G₁ to G₄. On the other hand Figure SI 3 compares the electrochemistry of a graphite powder (MCMB) with a model graphite single crystal electrode (HOPG) used for STM experiments. Both CVs show the same features, however it should be mentioned that a different potential sweep rate was used in both cases resulting in slight differences of the CVs. The differences between Figure SI 2 and SI 3 (a) are due to the fact that the first cycle typically is slightly different from the subsequent cycles, mainly due to SEI formation.

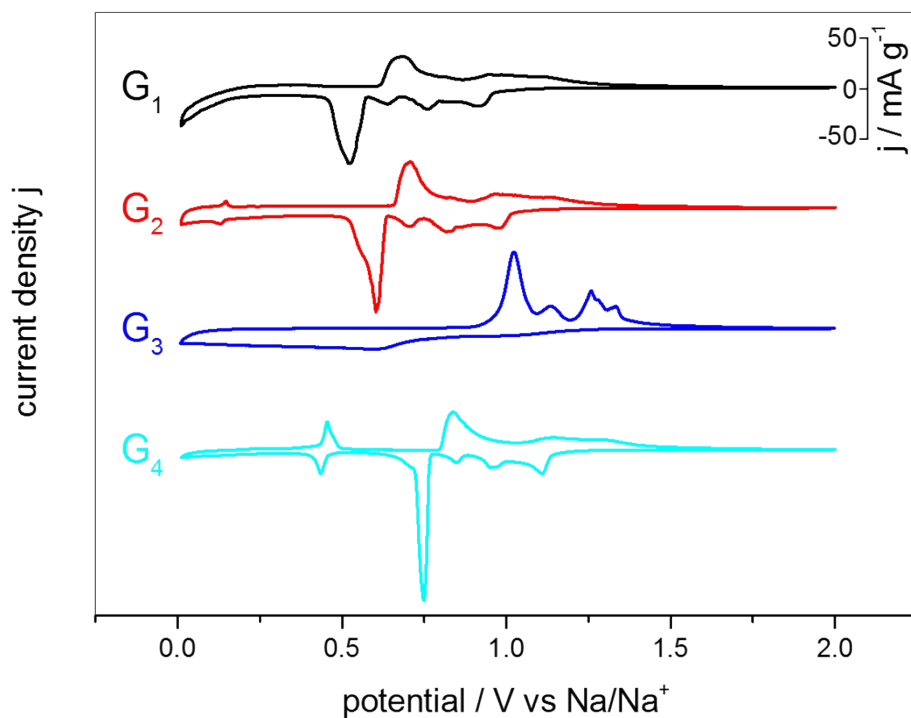


Figure SI 2: CVs of MCMB in 1 M NaClO₄ in G₁, G₂, G₃ and G₄ (sweep rate: 50 μV s⁻¹).

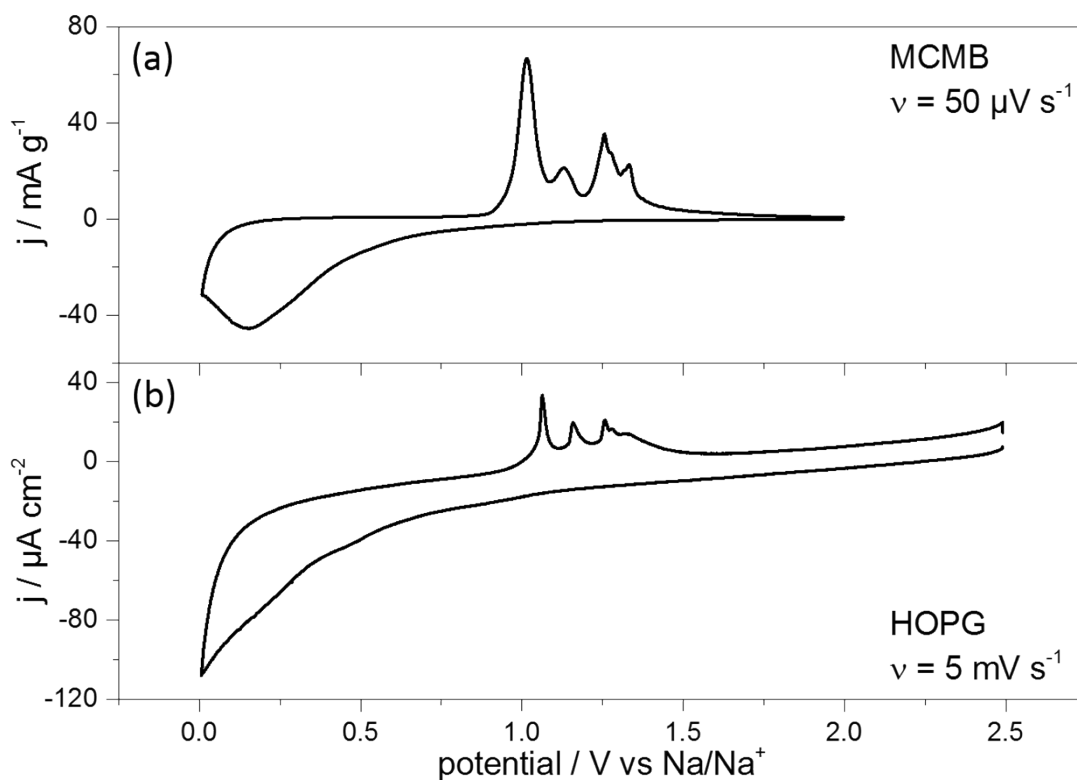


Figure SI 3: Comparison of the first CV cycles in 1 M NaClO₄ in G₃ of (a) a graphite powder (MCMB) with (b) a graphite single crystal (HOPG).

2.2. *In-operando* XRD

Figure SI 4 (a) shows the full data of the *in-operando* XRD over the full 2θ -range from 10° to 70° measured on MCMB electrodes immersed in 1 M NaClO₄ dissolved in G₁, G₂, G₃ and G₄. It also shows the data recorded over several charge/discharge cycles, where the corresponding potential data is shown in Figure SI 4 (b).

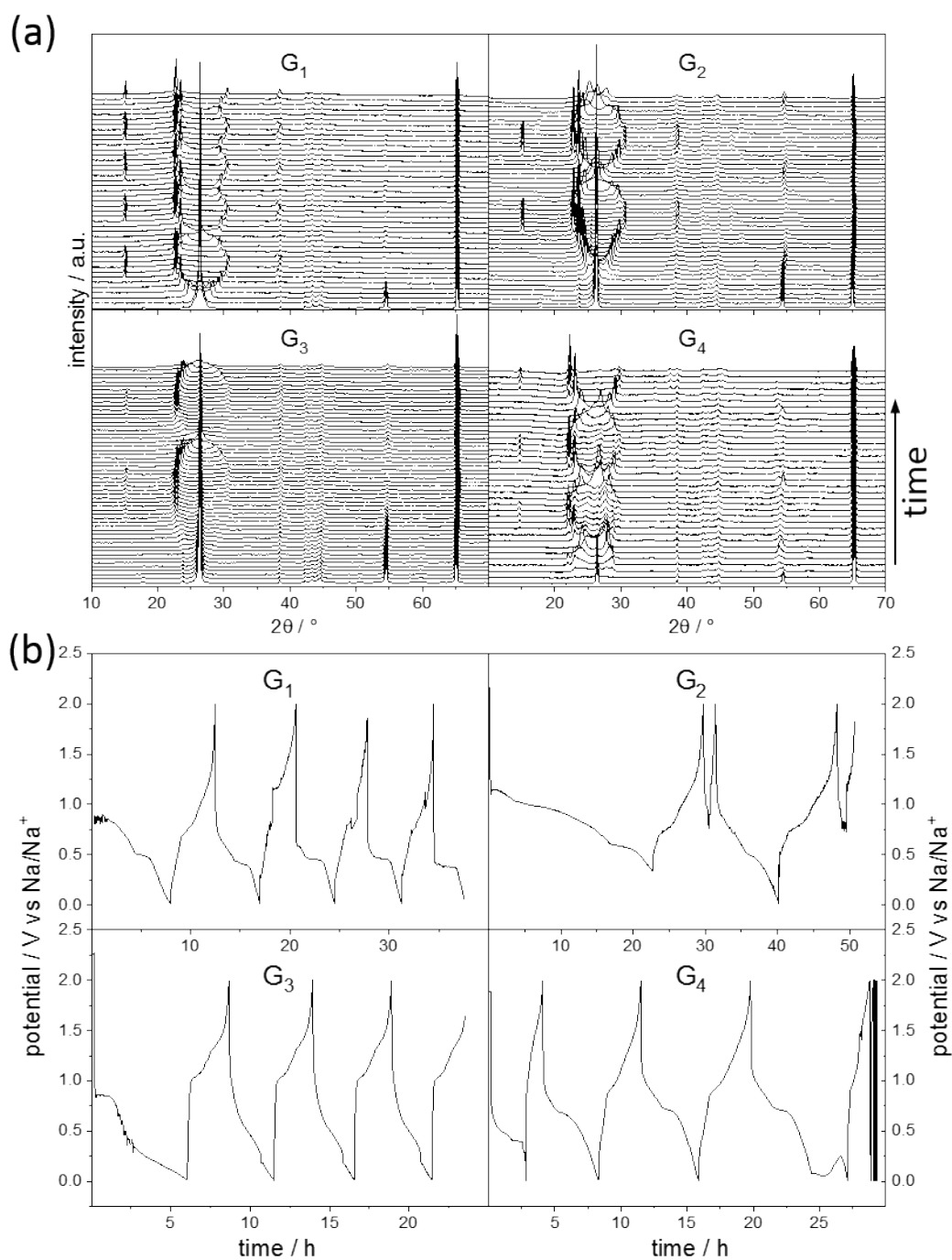


Figure SI 4: (a) Full XRD data set of the MCMB electrode in 1 M NaClO₄ in the different glymes and (b) the corresponding charge/discharge profiles.

For comparison Figure SI 5 (a) shows *in-operando* XRD data of a graphite electrode in a classical, carbonate-based electrolyte, namely 1 M NaClO₄ in EC/DMC (1:1), plus the corresponding charge/discharge profiles in Figure SI 5 (b). During the first discharge (intercalation) a reasonable amount of charge can be achieved, as can be seen from the long time until the lower cut-off voltage is reached. This charge is related to the irreversible SEI-formation, since it does not occur in the consecutive cycles. SEI formation of course does not result in any phase transition of the graphite crystals. Also in the consecutive cycles no change in the graphite lattice is observed. Moreover, the obtained small capacities clearly indicate that no Na-intercalation takes place.

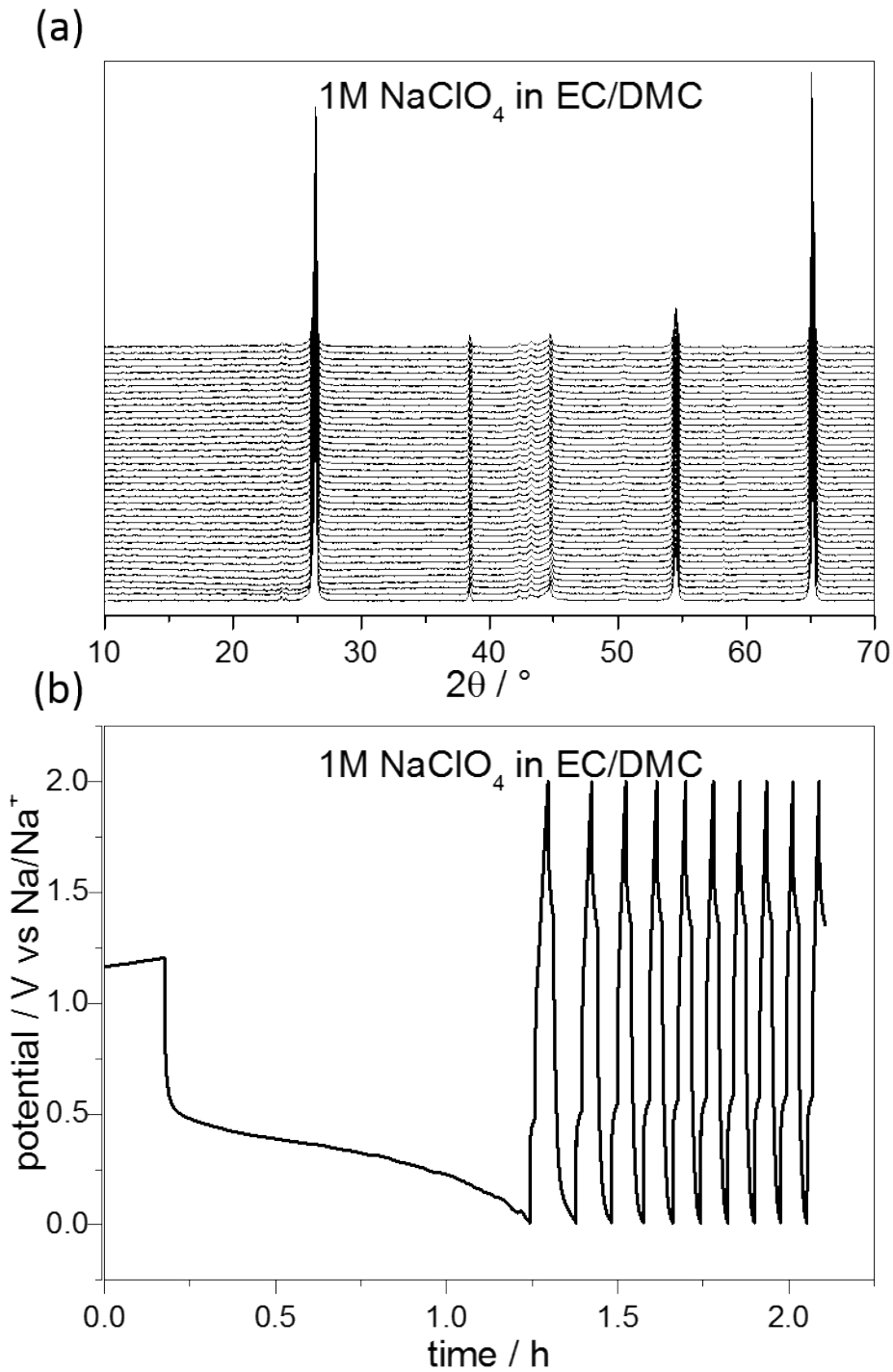


Figure SI 5: (a) Full XRD data set of the MCMC electrode in 1 M NaClO₄ in EC/DMC (1:1) and (b) the corresponding charge/discharge profiles.

Figure SI 6 shows the peak position of the XRD diffractograms measured in Figure SI 4 plotted against the time. At the same time the graph also shows the charge/discharge profile, allowing to directly relate electrochemistry and the phase transitions observed by XRD. Applying Bragg's law (Formula 2 in the main document), one can calculate the Miller indices h and also plot it versus time and relate it to electrochemistry (Figure SI 7).

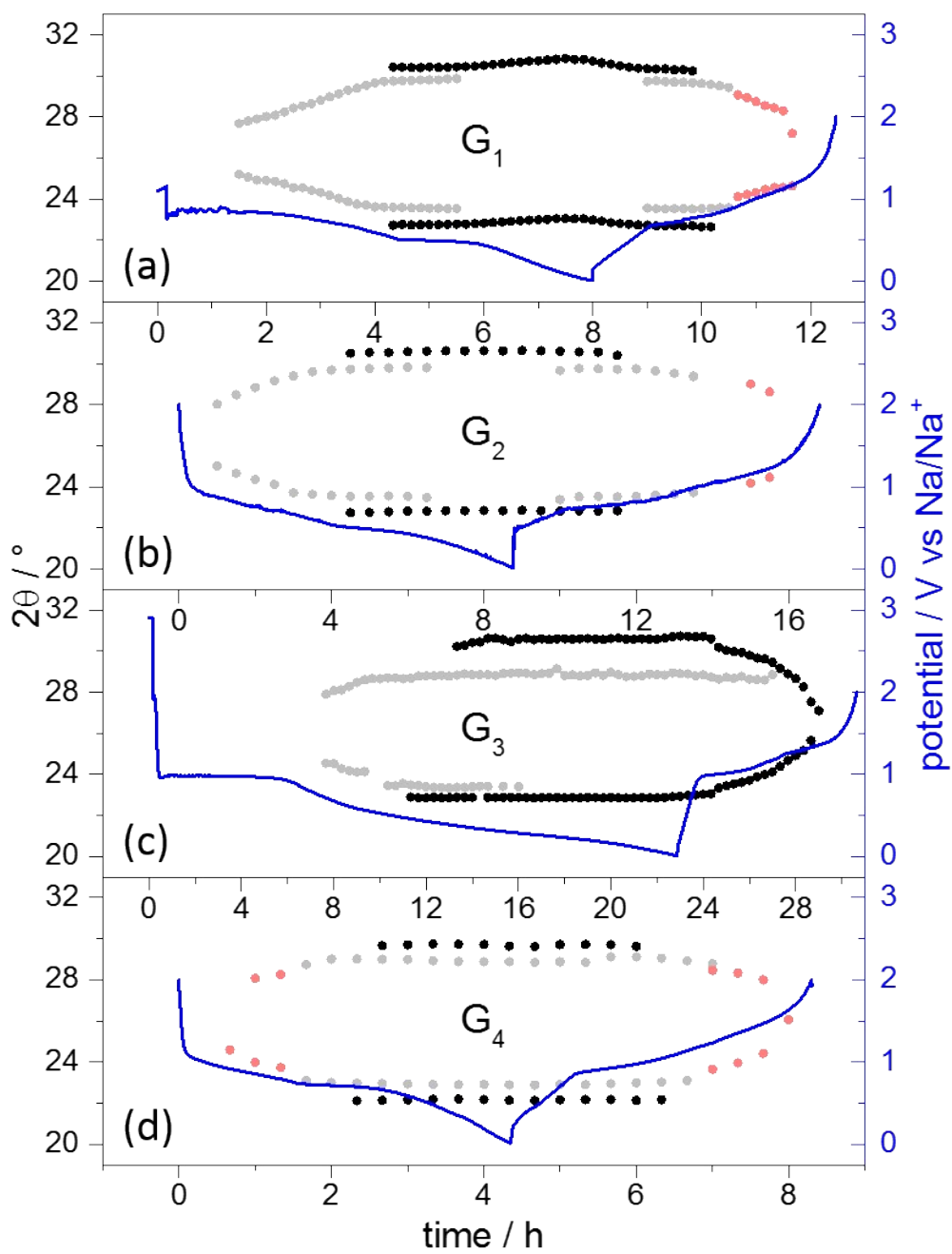


Figure SI 6: XRD peak positions and electrode potential plotted against the charge/discharge time measured on a MCMB electrode in 1 M NaClO_4 in (a) G_1 , (b) G_2 , (c) G_3 und (d) G_4 .

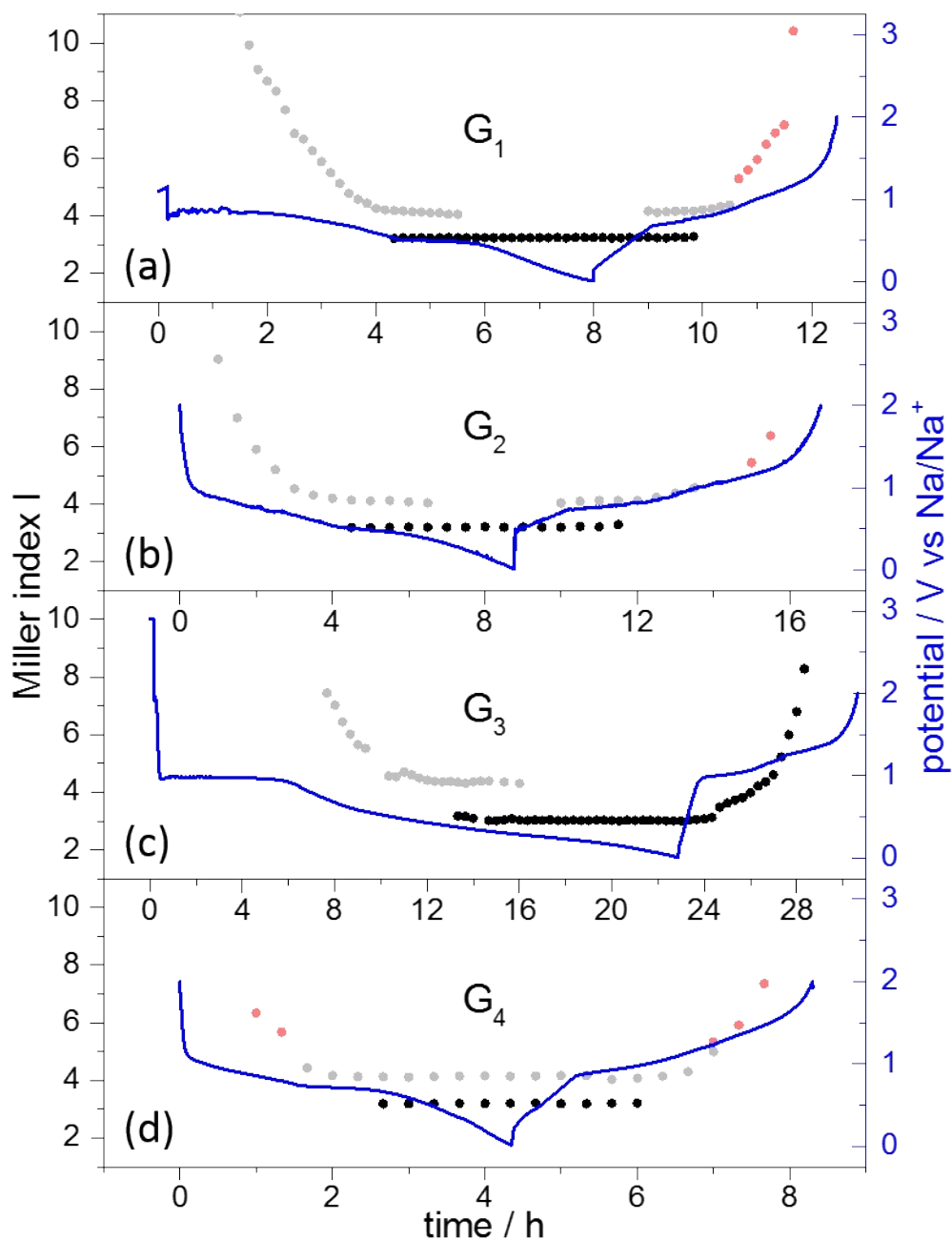


Figure SI 7: Miller index I of the ternary Na-GICs formed during sodiation and electrode potential plotted against the charge/discharge time measured on a MCMB electrode in 1 M NaClO_4 in (a) G_1 , (b) G_2 , (c) G_3 und (d) G_4 .

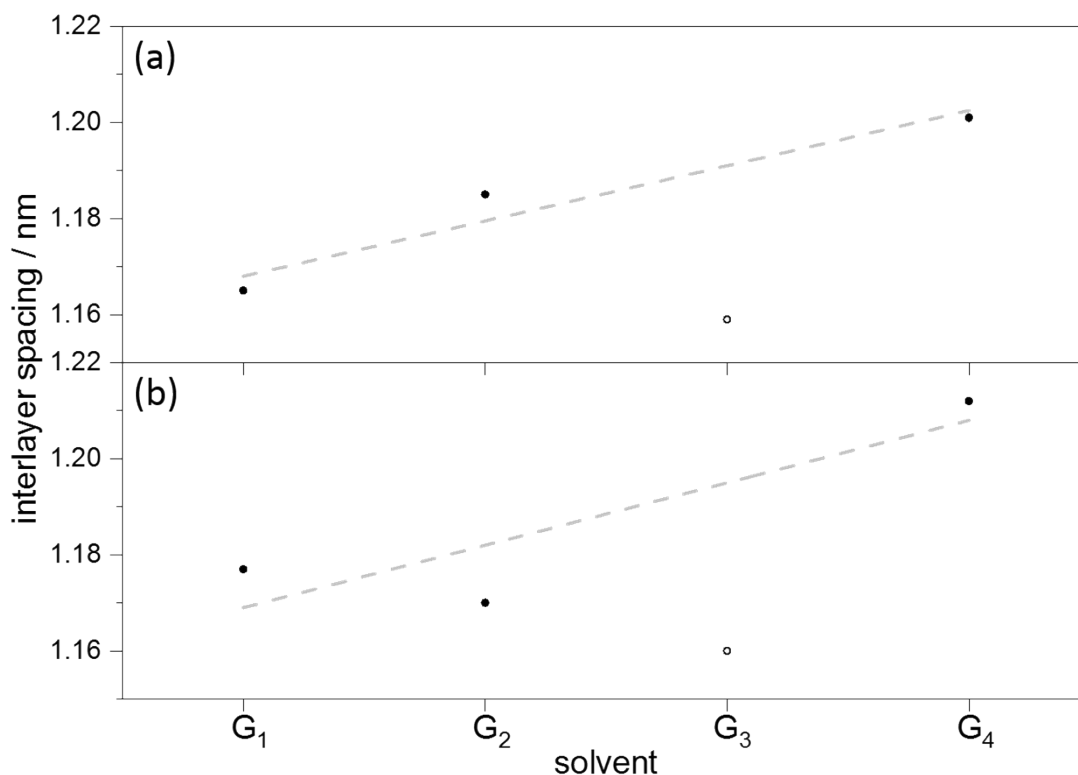


Figure SI 8: Interlayer spacing in between two sodiated graphene layers as a function of the solvent molecule of (a) the fully sodiated stage 1 Na-GIC and (b) the “half” sodiated intermediate stage 2 Na-GIC.

In order to determine the staging number n of the Na-GIC formed in the G₃-electrolyte, similar to the work by Kim *et al.* for G₂, an experiment with an HOPG chip was conducted, which was fully sodiated by bringing its edge face into contact with Na-metal (Figure SI 9). A physical contact without any electrolyte does not have any effect on the HOPG, which has an initial thickness of 0.8 mm and a weight of 0.1865 g (Figure SI 9 (a) and (b)). As soon as electrolyte (1 M NaClO₄ in G₃) is added into the gap between HOPG and Na, the HOPG starts to swell up, since one basically builds a short cut between the metallic Na negative electrode and the graphite positive electrode. In contrast to a similar experiment of Kim *et al.*⁴ in a G₂-electrolyte, sodiation proceeds significantly slower, *i.e.* within more than 20 minutes instead of only 3 minutes, being a hint for a slower Na⁺-diffusion inside the graphite lattice. After the swelling of the HOPG stopped, it had increased its thickness to 2.4 mm and the weight increased to 0.2912 g (Figure SI 9 (c) and (d)).

Upon full sodiation, the lattice constant of the graphite in the G₃-electrolyte amounts to 11.59 Å. The interlayer spacing for pristine graphite is 3.35 Å. Following the reasoning of Kim *et al.*, the lattice constant for a stage 1 Na-GIC, would correspond to the distance between two graphene layers with solvated Na ions inserted in between. Thus, one would expect a volume expansion by a factor of $11.59 \text{ Å} / 3.35 \text{ Å} = 3.46$. For a stage 2 Na-GIC, the lattice constant would correspond to sum of the spacings for one un-intercalated and one intercalated layer, so that the according expansion factor would be $11.59 \text{ Å} / (3.35 + 3.35) \text{ Å} = 1.73$, assuming that the empty graphene layers do not change thickness upon sodiation of neighbouring layers. The experimentally observed volume expansion amounts to $2.4 \text{ mm} / 0.8 \text{ mm} = 3$, which is pretty close to the theoretical value expected for a stage 1 Na-GIC. Thus, it is concluded that graphite forms a stage 1 Na-GIC when operated in the G₃-electrolyte.

From the weight of the HOPG chip before and after sodiation, one can also determine the number of coordinating G₃-molecules in the Na⁺(G₃)-complexes. The molecular weight of the Na⁺(G₃)₁-complex

amounts to $201.22 \text{ g mol}^{-1}$, of the $\text{Na}^+(\text{G}_3)_2$ -complex to $379.45 \text{ g mol}^{-1}$ and of the $\text{Na}^+(\text{G}_3)_3$ -complex to $557.68 \text{ g mol}^{-1}$. Intercalated into graphite (NaC_{30}), the $\text{Na}(\text{G}_3)_1\text{C}_{30}$ -compound has a molar weight of $561.55 \text{ g mol}^{-1}$, the $\text{Na}(\text{G}_3)_2\text{C}_{30}$ -compound of $739.78 \text{ g mol}^{-1}$ and the $\text{Na}(\text{G}_3)_3\text{C}_{30}$ -compound of $918.01 \text{ g mol}^{-1}$. The pristine C_{30} has a molar mass of $360.11 \text{ g mol}^{-1}$. Thus, the mass ratios between pristine and sodiated graphite are 0.64 in case of the $\text{Na}^+(\text{G}_3)_1$ -complex, 0.49 for the $\text{Na}^+(\text{G}_3)_2$ -complex and 0.39 for the $\text{Na}^+(\text{G}_3)_3$ -complex. The measured mass ratio of the HOPG chip before and after sodiation amounts to $0.1865 \text{ g} / 0.2912 \text{ g} = 0.64$. Thus, it is clear that the Na-ions are coordinated by only one G_3 -molecule upon intercalation.

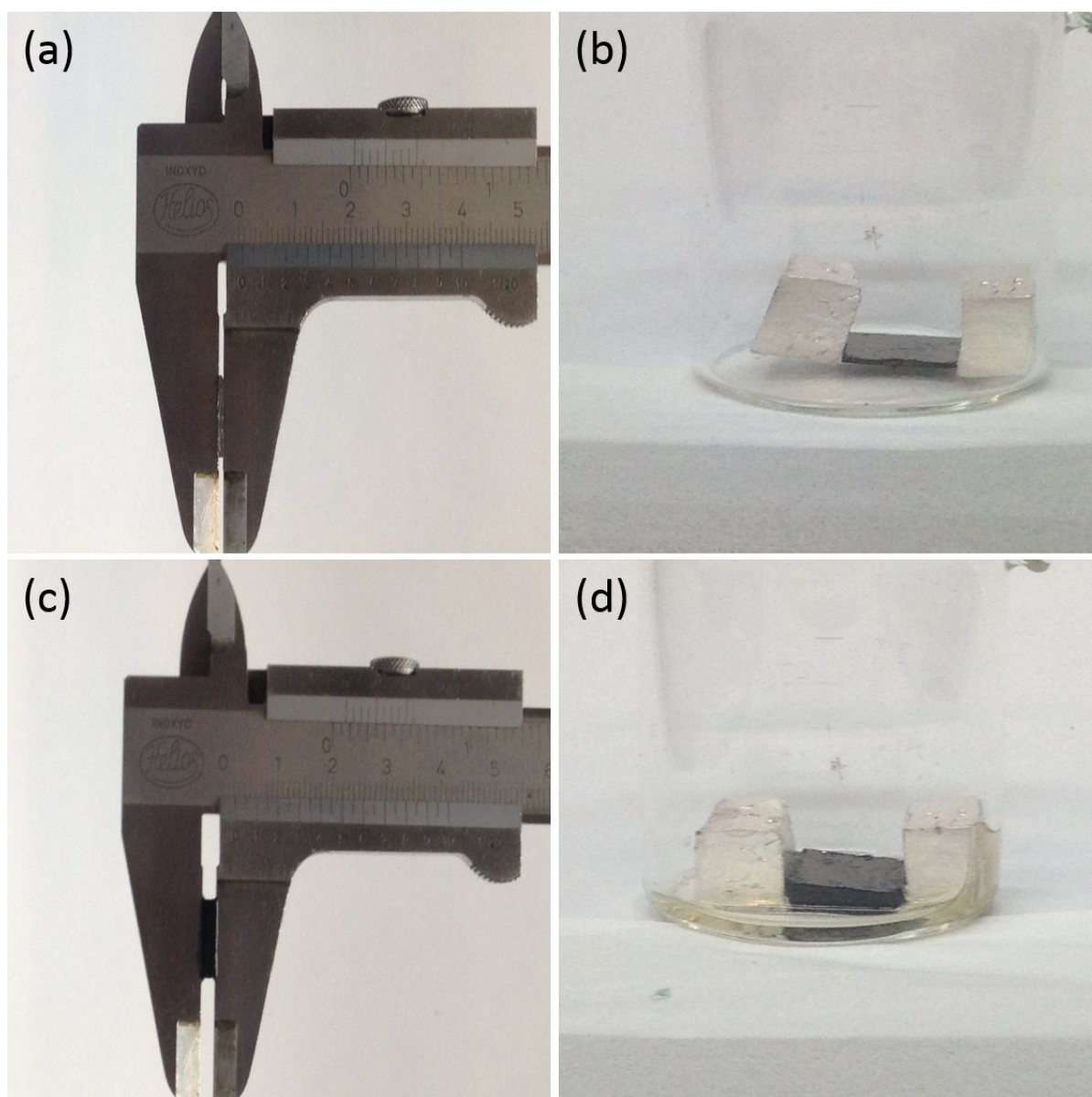


Figure SI 9: Sodiation of an HOPG chip in the 1 M NaClO_4 in G_3 electrolyte. (a) Pristine thickness of the original HOPG chip (0.8 mm) and the experimental setup in (b) with two Na-blocks touching the open HOPG facets in absence of an electrolyte. Adding the electrolyte results in a volume expansion of the HOPG sample to 2.4 mm (c) as can also be seen by eye in direct comparison in the beaker cell (d).

2.3. *In-operando* EC-STM

Figure SI 10 shows a series of STM images recorded *in-operando*, while the potential of the HOPG electrode immersed in 1 M NaClO_4 in G_3 was varied. The corresponding voltammogram is shown in the

centre of the figure. Each STM image has a frame with the same colour as in the corresponding section of the CV, thus indicating the potential range in the CV during which the image was measured. Hence, the experiment starts with the black framed image on the right side in the lower row. The potential was ramped from the initial 2.5 V to 1.1 V, where the potential was held until the STM scan was completed. During the potential hold, the (absolute) current decreased, causing the vertical lines in the voltammogram. In the next step, the potential was further lowered to 0.75 V, where the potential sweep was paused again. The potential of the STM-tip was held constant at 2.6 V, meaning that the potential bias between sample and tip changed with the WE potential. The slight grey CV, which has an arbitrary unity here, is a CV measured with a powder MCMB electrode at a much lower sweep rate and serves as a reference and as a guide to the eye. Certain differences between the CV at HOPG and MCMB are expected, as the latter (powder) sample has many more possible intercalation sites compared to the HOPG sample.

Starting with the black framed image, which shows the pristine HOPG sample, one can see all the typical HOPG features as the largely extended, atomically flat terraces, being interrupted by atomic step edges crossing the image. In the present case, four step edges are visible, while the highest one, which is the second one counting from left, consists of five atom layers. As can be seen, the surface morphology remains unchanged and atomically smooth in that potential range. Also when the potential is further lowered to 0.75 V, as shown in the image with the red frame, no topographic changes are visible.

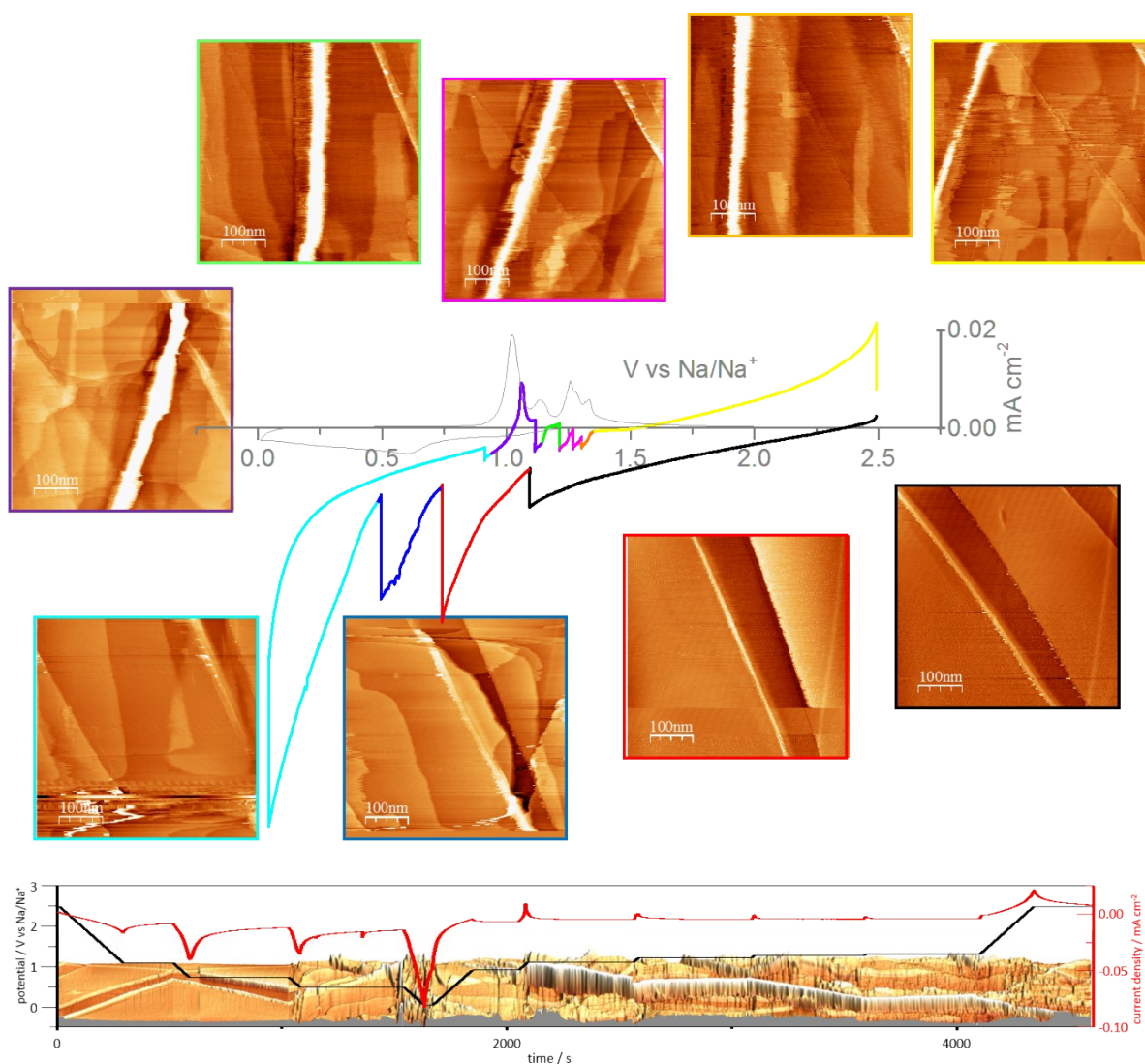


Figure SI 10: *In-operando* EC-STM of HOPG in 1M NaClO₄ in G₃. The HOPG surface was scanned by EC-STM (tunnelling current: 8 nA, scan rate: 1 Hz, tip potential: 2.6 V, bias potential: variable), while a CV (sweep rate: 5 mV s⁻¹) was measured simultaneously. The colours of the frame around the STM-images indicates the potential range, which was applied during imaging, and corresponds to the colours used in the CV. The light grey CV (sweep rate: 50 μV s⁻¹) corresponds to a MCMB electrode measured in a Swagelok® cell and serves as a reference. The figure on the bottom is the 3D representation of the *in-operando* EC-STM plotting the measured horizontal lines in the individual figures versus the total time of the experiment rather than the y-axis, and also shows the applied potential and measured electrochemical current.

This changes in the blue framed image, which was scanned from top to bottom and from 0.75 V to 0.5 V. In the very upper part some almost horizontal lines are visible. As already discussed in the main text, these lines originate from the insertion of the solvated Na-ions and the concomitant lattice expansion of the graphite (002)-plane, which is visible in real time here. A magnification of this image can also be found in Figure SI 11, where an exemplary analysis of the graphite interlayer spacing by means of height profiles is shown. In comparison to the previous red framed image, one can clearly see, how and where the intercalation takes place. The height data from the height profiles was used together with other data to determine the interlayer spacings in Table 2 in the main document.

Now, the potential was further lowered to 0.05 V and raised back to 0.9 V in the cyan coloured image. In the bottom part of that image, which is where the STM scan starts, some further phase transitions

are visible. As can be seen in the CV, the potential sweep was stopped shortly below the onset potential of Na-de-intercalation. Thus, the upper part of the cyan STM image, which was mainly measured during the anodic scan, does not show any phase transition.

The potential scan of the purple framed image (0.9 V to 1.12 V) was limited to the first de-intercalation peak. Again phase transitions are visible, however, this time the swellings disappear and the distance between the graphene layers reduces. Next, the green framed image (1.12 V to 1.22 V) was measured in the potential window of the second de-intercalation peak. Here, one can see a phase transition in the lower part of the image, where the potential was still swept. In the potential range of the pink image (1.22 V to 1.275 V), another transition is visible in the upper part, where again the potential was varied. The orange image was scanned in a potential range from 1.275 V to 1.31 V, which is in the range of the last de-intercalation peak. If one takes a close look to the lower left corner, one can make out another phase transition, which occurs in the range, where the potential was still varied. The last image (yellow) of this series shows the surface in the range from 1.31 V to 2.5 V. No obvious phase transitions are visible, since the de-intercalation should be completed at this stage. However, one can still see expanded terraces being a hint that some residue irreversibly remains in the graphite lattice.

Another noticeable observation of this STM series is that the image quality becomes poorer, especially after the sample was exposed to lower electrode potentials. This can be seen in the 3D representation of the same series in the bottom part of Figure SI 10. Since in STM the sample is scanned line by line with a certain frequency, one can assign a time to each pixel, which itself can be matched with the time of the potential scan in the CV. Thus, one can link the electrode morphology to the electrode potential, which proved to be a powerful technique for similar studies on the SEI-formation on HOPG in LIBs.⁵ As one can see, the electrode roughness increases when the potential is in the range of 0.5 V and below. This surface roughness remains throughout the entire experiment, also at higher potentials and causes the fuzziness in the STM images.

Figure SI 11 illustrates the method, how the lattice expansions upon sodiation/desodiation of the graphite are determined. Height profiles are measured across the features representing phase transitions. In order to obtain the lattice interlayer spacing, one has to take into account that by the height profiles only the additional lattice expansion upon sodiation is measured, neglecting the original 3.35 Å. Thus, in order to determine the interlayer spacing, which is also obtained from XRD, the 3.35 Å have to be added to the measured height of the phase transition. The values presented in Table 2 in the main document are based on a statistical analyses, while a set of ca. 50 phase transitions was analysed.

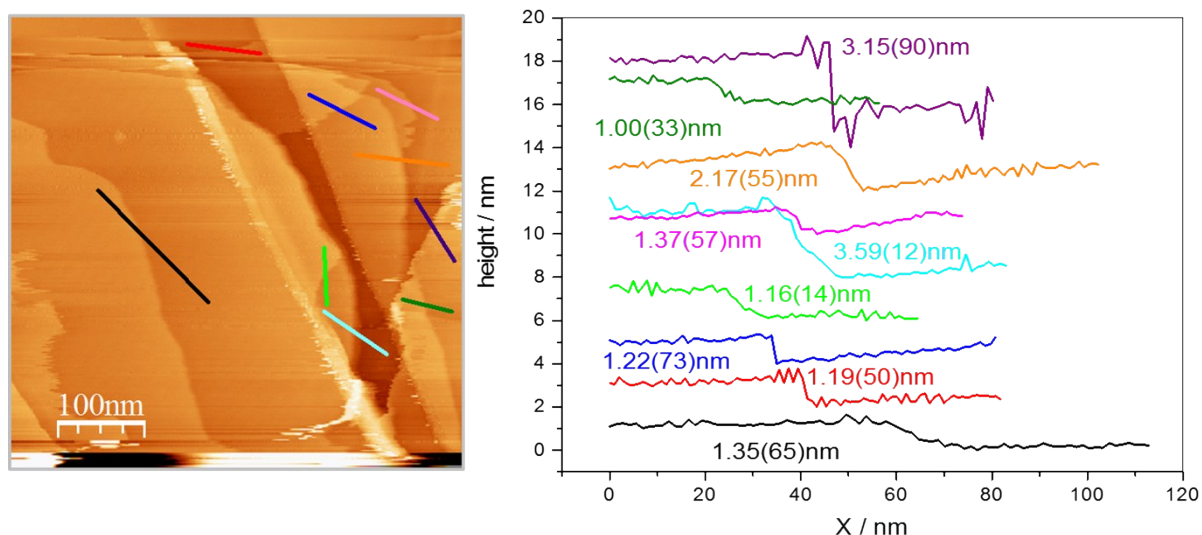


Figure SI 11: Height profile analysis for the statistical evaluation of the graphite lattice expansion during sodiation measured by STM of HOPG in 1 M NaClO₄ in G₃.

In the next set of experiments, the solvent G₄ was used instead of G₃ and the Na-intercalation behavior was again studied by STM. As before, Figure SI 12 shows the HOPG surface in dependence of the applied electrode potential. The potential was scanned continuously during this experiment, without potential hold. The yellow as well as the black framed image were both recorded at potentials above the intercalation regime, where both images show plenty of step edges interrupting the atomic planes. The red framed image, which covers the entire intercalation regime, still shows the flat terraces in the lower fifth of the image, which was recorded at higher potentials. Then, the STM image seems to be disturbed, however, taking a close look one recognizes numerous phase transitions. These transitions can be found throughout the entire image and are not as clearly defined as in the upper case with the G₃ electrolyte.

Also during the anodic sweep, where the blue framed image was measured, various phase transitions are visible. In the low potential regime of the image, which is the upper part, intercalation phase transitions can be observed, while in the high potential regime in the lower part of the image, de-intercalation phase transitions can be found. The bright horizontal line in the lower third seems to be the border between intercalation and de-intercalation. Phase transitions observed before this horizontal line are intercalation phase transitions, while afterwards they are caused by de-intercalation. The cyan framed image shows plenty of de-intercalation phase transitions in its lower part, which was also recorded at lower potential, while the number of phase transitions becomes smaller at higher potentials. In the purple framed image one can finally find only a minor amount of phase transitions.

Comparing the first (black) and the last image (purple) of this STM series, one can see that the sample topography changes a lot during the potential cycle. The imaged position is still almost the same, as can be seen from the diagonal step edge crossing the image from the lower left corner to the upper right corner. However, it seems as if some previously present step edges are missing or at least are no longer visible. Moreover, as also observed in the case of G₃, some irreversibly remaining species are still present in the graphite lattice.

Also here, one can plot the entire experiment in 3D and overlay it with the applied potential and the correlating current, as is shown in the lower part of Figure SI 12. This plot again indicates a surface film formation at low potentials close to 1.0 V. In the course of this experiment, this film seems to disappear

again, even though it is also visible at high potentials in the beginning. It seems as if the surface film disappears slowly with time.

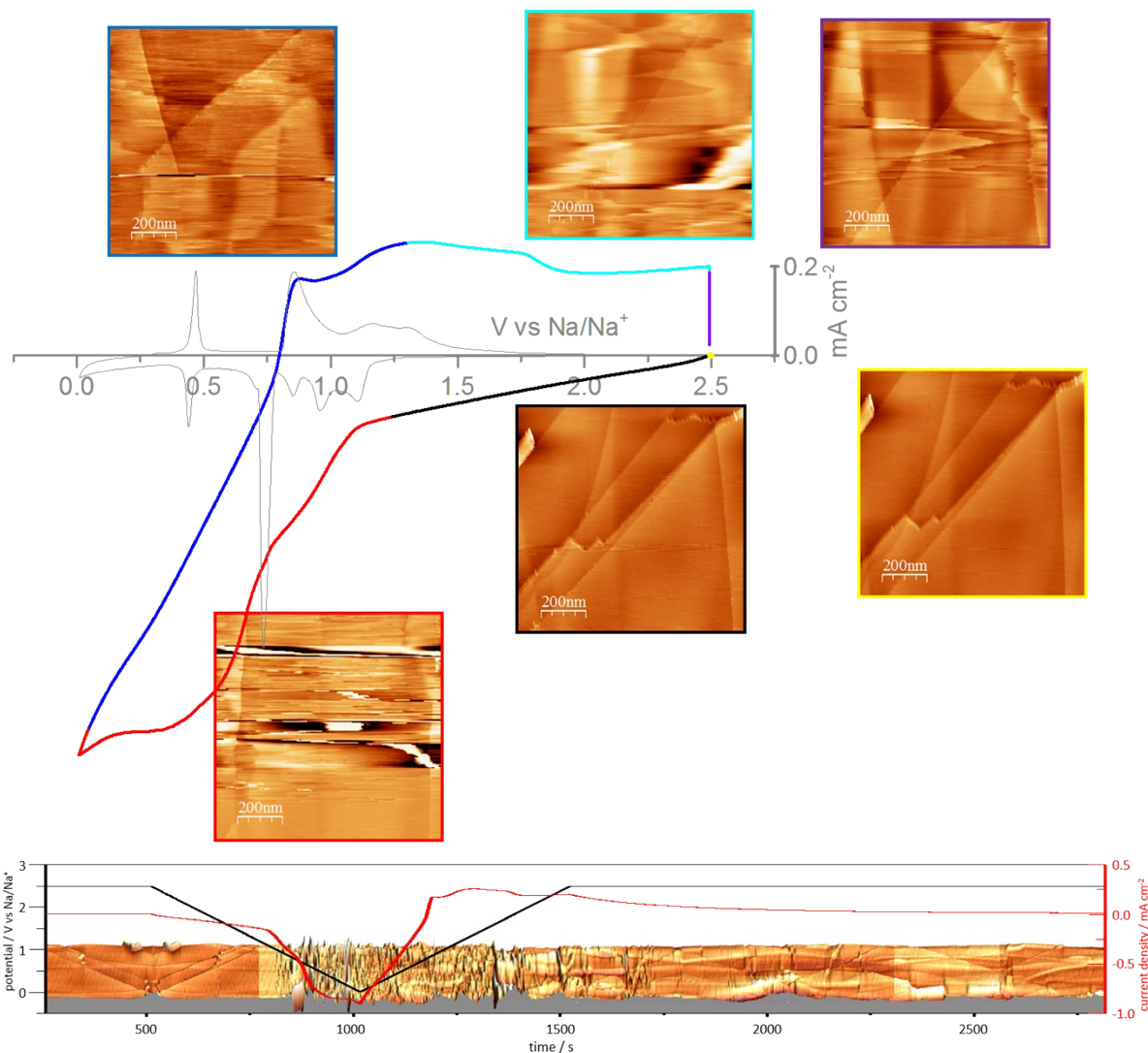


Figure SI 12: *In-operando* EC-STM of HOPG in 1M NaClO₄ in G₄. The HOPG surface was scanned by STM (tunnelling current: 1 nA, scan rate: 1 Hz, tip potential: 2.6 V, bias potential: variable), while a CV (sweep rate: 5 mV s⁻¹) was measured simultaneously. The colours of the frame around the STM-images indicate the potential range, which was applied during imaging and which corresponds to the colours used in the CV. The light grey CV (sweep rate: 20 μV s⁻¹) corresponds to a MCMB electrode measured in a Swagelok® cell and serves as a reference. The figure on the bottom is the 3D representation of the *in-operando* EC-STM.

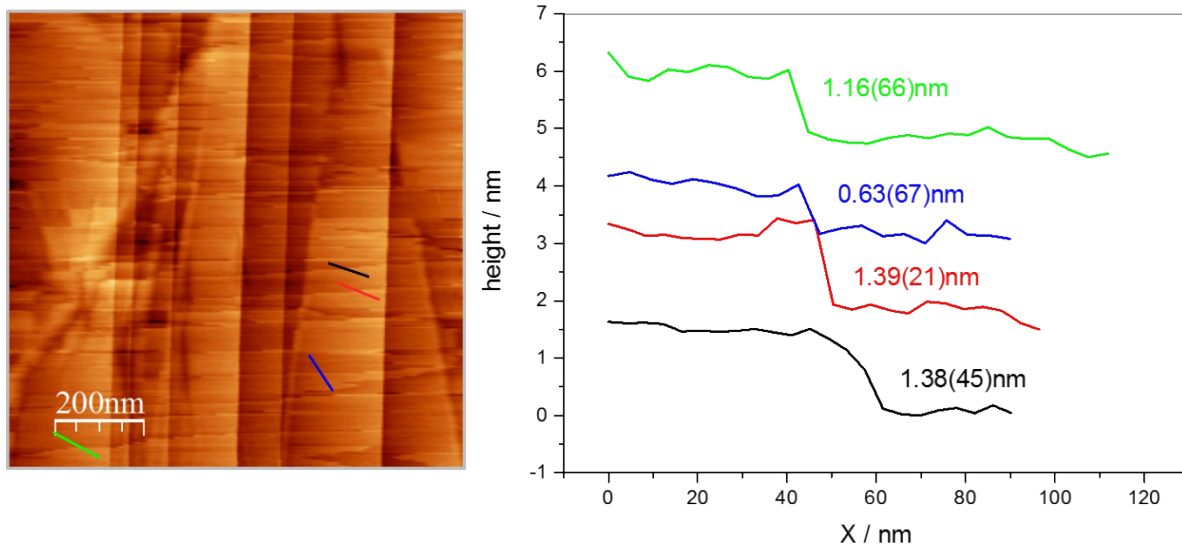


Figure SI 13: Height profile analysis for the statistical evaluation of the graphite lattice expansion during sodiation measured by STM of HOPG in 1 M NaClO₄ in G₄.

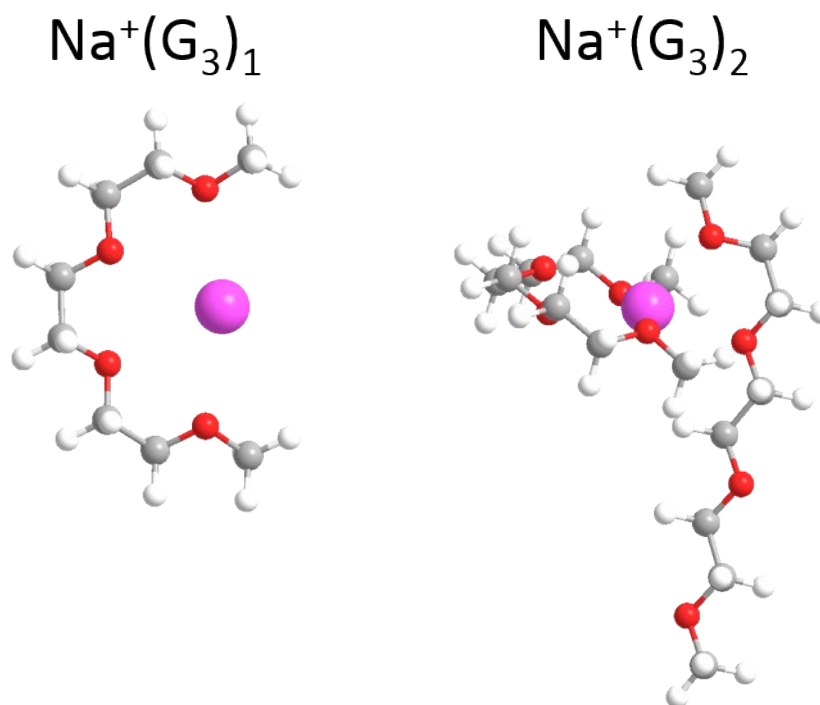


Figure SI 14: Ball-stick models of the under-coordinated Na⁺(G₃)₁-complex (CN 4) and the over-coordinated Na⁺(G₃)₂-complex (CN 8). (pink: Na⁺, red: O-atom, grey: C-atom, white: H-atom)

Figure SI 14 shows two possible Na⁺(G₃)-geometries. From a simple evaporation experiment, in which a drop (100 μl) of the 1 M NaClO₄ in G₃ electrolyte was weighed, exposed to vacuum for several days and weighed again, the number of coordinating G₃-molecules can be estimated, since it is believed that all the unbound G₃-molecules in the droplet evaporate and only the coordinated Na⁺(G₃)-complexes remain. The Na⁺(G₃)₁-complex is found to be the more probably geometry. The idea behind this evaporation experiment is that the Na⁺(G_x)_y-complexes behave like a solvated ionic liquid, which is well known for glyme-coordinated alkali ions.^{6, 7} Similar to real ionic liquids, solvated ionic liquids have a very low vapour pressure and do not evaporate in vacuum. Thus, by exposing a 1 M NaClO₄ solution in glyme solvent to vacuum removes the excess glyme molecules and a clear droplet with decreased size remains. From its weight, the upper mentioned solvation structure can be determined.

This result is in agreement with the mass change of the HOPG single crystal chip during the experiment shown in Figure SI 9.

2.4. In-operando EQCM

Set of equations for the Daikhin model:

$$q_0 = (i 2\pi n f_0 \rho / \eta)^{1/2} \quad (\text{SI 1})$$

$$q_1^2 = q_0^2 + \xi^{-2} \quad (\text{SI 2})$$

$$W = q_1 \cdot \cosh(q_1 h) + q_0 \cdot \sinh(q_1 h) \quad (\text{SI 3})$$

$$dW_{film}/n = -\frac{4f_0^2 \rho}{(\mu_q \rho_q)^{1/2}} \text{Im} \left\{ \frac{1}{q_0} + \frac{h}{\xi^2 q_1^2} - \frac{1}{W} \frac{1}{\xi^2 q_1^2} \left[\frac{2q_0}{q_1} [\cosh(q_1 h) - 1] + \sinh(q_1 h) \right] \right\} \quad (\text{SI 4})$$

$$df_{film}/n = -\frac{2f_0^2 \rho}{(\mu_q \rho_q)^{1/2}} \text{Re} \left\{ \frac{1}{q_0} + \frac{h}{\xi^2 q_1^2} - \frac{1}{W} \frac{1}{\xi^2 q_1^2} \left[\frac{2q_0}{q_1} [\cosh(q_1 h) - 1] + \sinh(q_1 h) \right] \right\} \quad (\text{SI 5})$$

$$\frac{df}{n} = df_{film} (1 - m\pi r^2) q - \frac{3}{2} \frac{f_0^2 \rho \delta_n}{(\rho_q \mu_q)^{1/2}} m r^2 \frac{\pi^2}{2} - \frac{4}{3} \frac{f_0^2 \pi r^3}{(\rho_q \mu_q)^{1/2}} m (\rho_b + \rho) - (1 - q) \frac{2f_0^2 \rho}{(\rho_q \mu_q)^{1/2}} \text{Re} \quad (\text{SI 6})$$

$$\frac{dW}{n} = dW_{film} (1 - m\pi r^2) q + \frac{3f_0^2 \rho \delta_n}{(\rho_q \mu_q)^{1/2}} m r^2 \frac{\pi^2}{2} - (1 - q) \frac{4f_0^2 \rho}{(\rho_q \mu_q)^{1/2}} \text{Im} \left(\frac{1}{q_0} \right) \quad (\text{SI 7})$$

With the overtone number n , the resonance frequency f_0 of the coated quartz in outside the electrolyte, the gravimetric density ρ of the electrolyte and its viscosity η . ξ and h are roughness parameters (lateral and vertical, respectively). μ_q and ρ_q are the crystal shear modulus and the density of the quartz. m denotes the particle density on the quartz surface with a relative surface coverage q of the quartz and a particle radius r . The gravimetric density of the particles is described by ρ_b . The variable penetration depth δ_n of the shear wave emitted by the oscillating quartz crystal towards the electrolyte is given by $\delta_n = \sqrt{\eta/\pi n f_0 \rho}$.

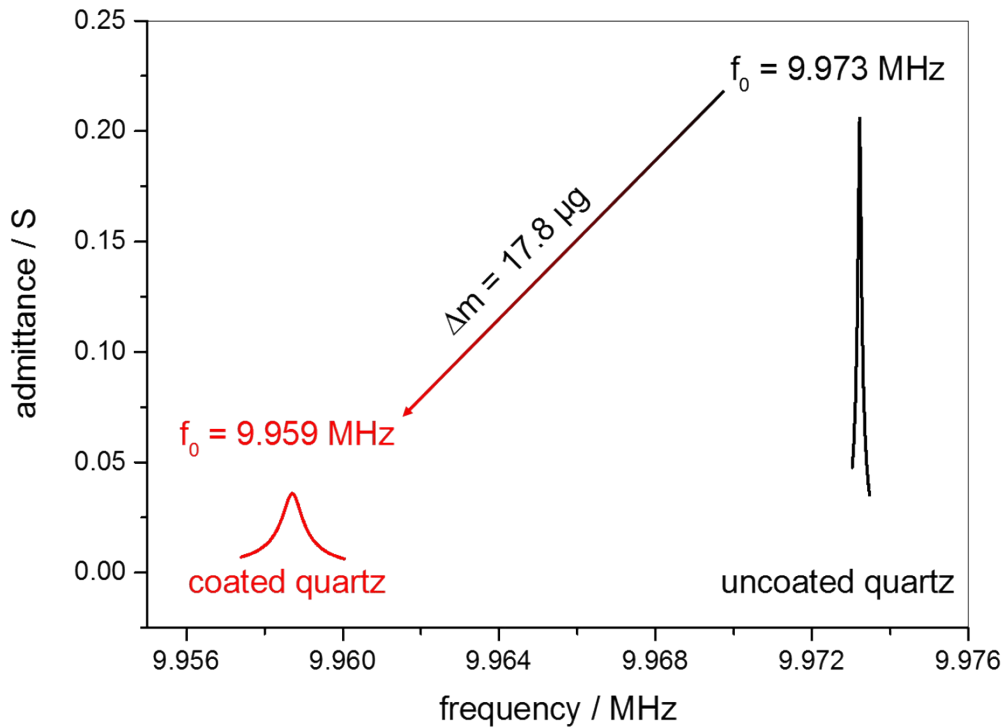


Figure SI 15: Effect of the electrode coating on the resonance frequency f_0 of the oscillating quartz. Both resonance curves are measured in air before (black) and after (red) coating the quartz with SFG6 graphite. According to Sauerbrey a frequency shift of $df = 14$ kHz is equivalent to a mass loading of $\Delta m = 17.8 \mu\text{g}$.

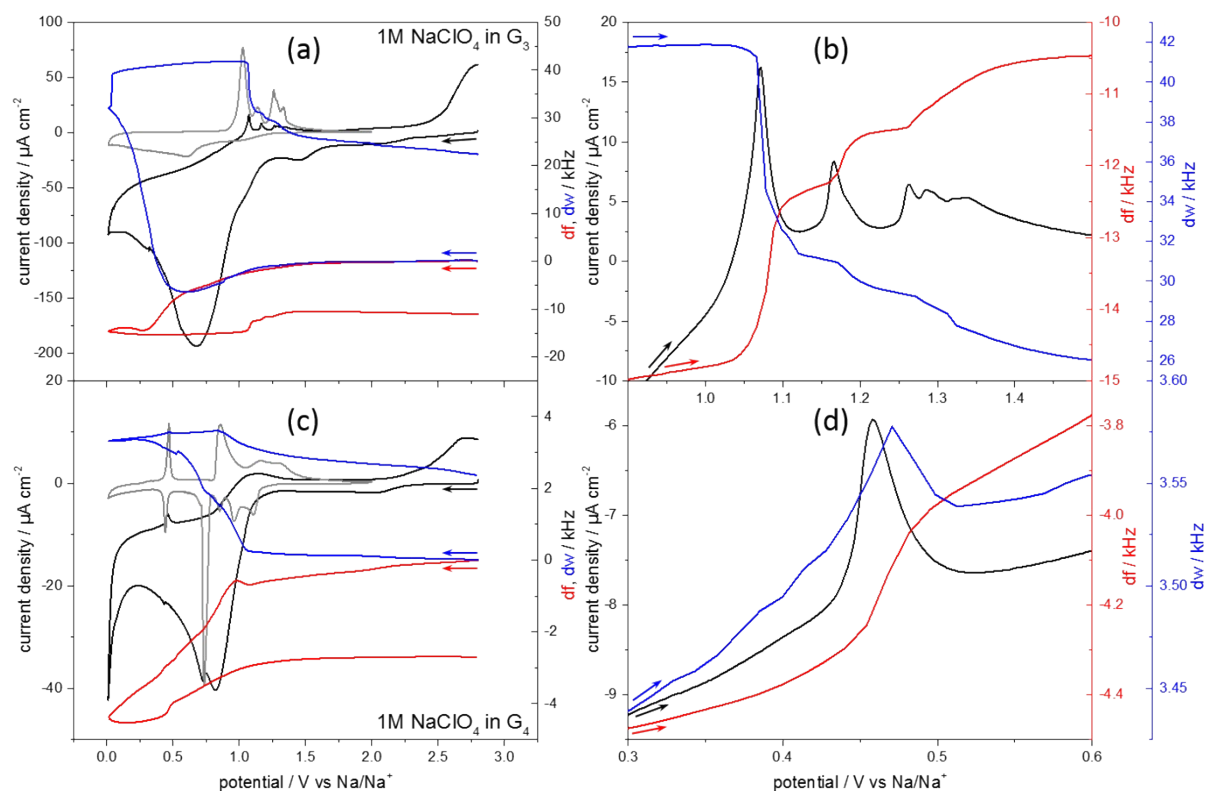


Figure SI 16: In-operando EQCM of SFG6 graphite coated on an Au-quartz in 1M NaClO₄ in (a) G₃ with (b) a magnification of the desodiation regime and in (c) G₄ with (d) a magnification of the low potential desodiation peak (sweep rate: 2 mV s⁻¹). The light grey CV (sweep rate: 20 $\mu\text{V s}^{-1}$) corresponds to a MCM electrode measured in a Swagelok[®] cell and serves as a reference, while the current scale is arbitrary.

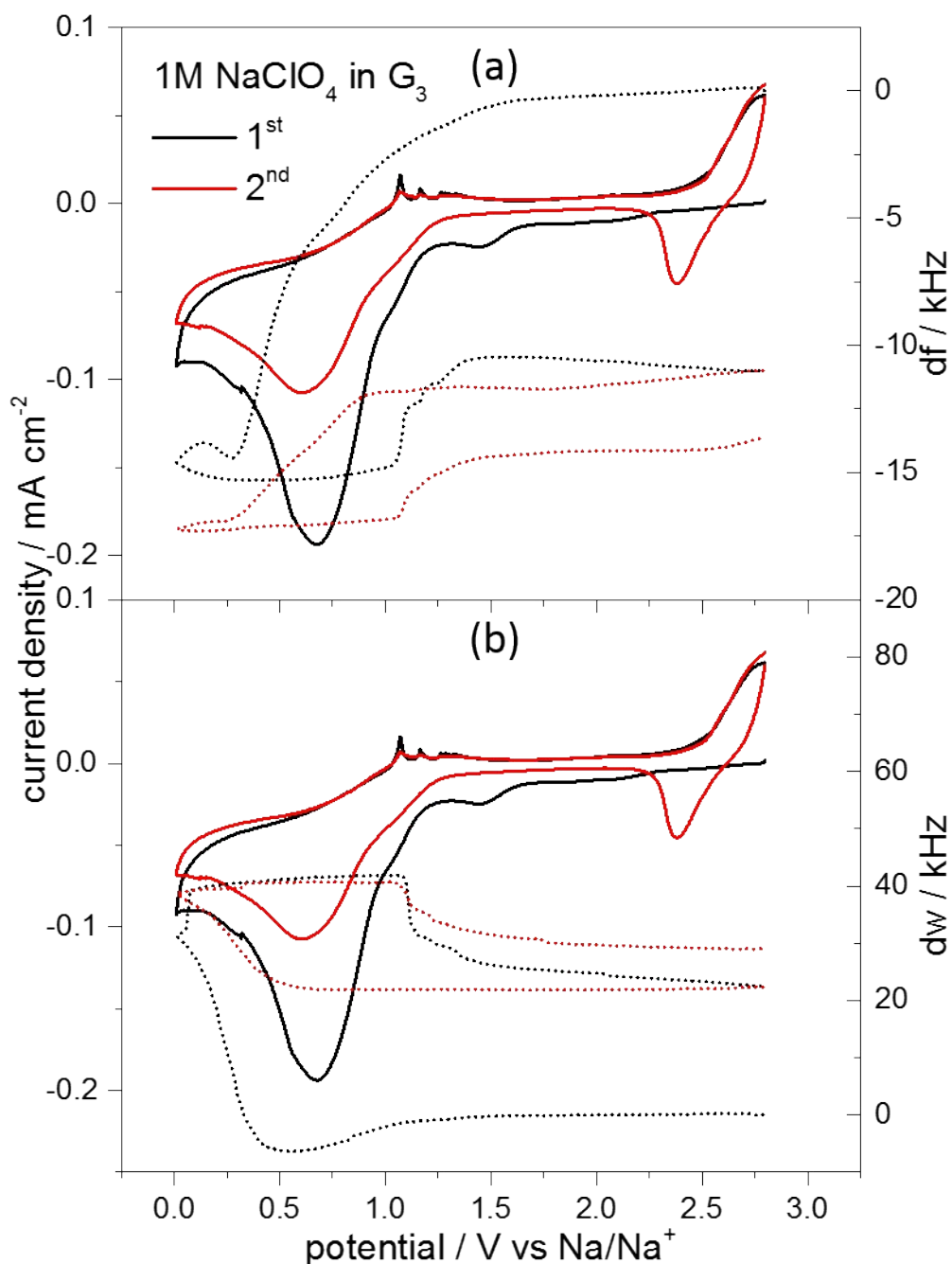


Figure SI 17: EQCM data of the first two cycles of a graphite coated Au-quartz in 1 M NaClO₄ in G₃ with the change of resonance frequency df shown in (a) and the change of damping dw shown in (b).

References

- 1 S. Hartung, N. Bucher, R. Bucher and M. Srinivasan, *Rev. Sci. Instrum.*, 2015, **86**, 86102-1-86102-3.
- 2 I. Horcas, R. Fernández, J. M. Gómez-Rodríguez, J. Colchero, J. Gómez-Herrero and A. M. Baro, *Rev. Sci. Instrum.*, 2007, **78**, 13705.
- 3 G. Sauerbrey, *Zeitschrift für Phys.*, 1959, **155**, 206-222.
- 4 H. Kim, J. Hong, G. Yoon, H. Kim, K.-Y. Park, M.-S. Park, W.-S. Yoon and K. Kang, *Energy*

- Environ. Sci.*, 2015, **8**, 2963–2969.
- 5 L. Seidl, S. Martens, J. Ma, U. Stimming and O. Schneider, *Nanoscale*, 2016, **8**, 14004–14014.
- 6 K. Ueno, K. Yoshida, M. Tsuchiya, N. Tachikawa, K. Dokko and M. Watanabe, *J. Phys. Chem. B*, 2012, **116**, 11323–11331.
- 7 T. Mandai, K. Yoshida, K. Ueno, K. Dokko and M. Watanabe, *Phys. Chem. Chem. Phys.*, 2014, **16**, 8761–72.